1-1-2011

Spectroscopic and computational study of β-ethynylphenylene substituted zinc and free-base porphyrins

John C. Earles
Otago University

Keith C. Gordon
Otago University

Adam W. I Stephenson
Massey University

Ashton C. Partridge
Massey University

David L. Officer
University of Wollongong, davido@uow.edu.au

Spectroscopic and computational study of β-ethynylphenylene substituted zinc and free-base porphyrins

Abstract

A series of tetraphenylporphyrins appended at the β-pyrrolic position with an ethynylphenylene- or ethynylpyridine-substituent have been subjected to spectroscopic and density functional theory (DFT) analyses. The mean absolute deviation between corresponding experimental and DFT-derived vibrational spectra is up to 10.2 cm -1, suggesting that the DFT B3LYP/6-31G(d) method provides an accurate model of the β-substituted porphyrin systems. The configuration interactions that give rise to prominent electronic absorptions have been calculated using time-dependant DFT (TD-DFT) and have been rationalized with reference to the energy and topology of DFT calculated molecular orbitals. As the electron withdrawing capacity of the β-substituent increases the LUMO orbital gains appreciable amplitude over the substituent moiety and is stabilised. This represents a departure from the assumptions underpinning the Gouterman four-orbital model, resulting in atypical electronic absorption spectra. This phenomenon is also manifested in the enhancement patterns of the resonance Raman spectra insofar as B-band excitation engenders an enhancement of substituent based modes. These observations demonstrate that the β-substituent exerts an appreciable electronic influence on the porphyrin π-electron system and provides a means of introducing charge-transfer character to prominent electronic transitions. © 2011 the Owner Societies.

Keywords

spectroscopic, free, zinc, substituted, base, ethynylphenylene, porphyrins, study, computational, β

Disciplines

Life Sciences | Physical Sciences and Mathematics | Social and Behavioral Sciences

Publication Details

Earles, J. C., Gordon, K. C., Stephenson, A. W. I., Partridge, A. C. & Officer, D. L. (2011). Spectroscopic and computational study of β-ethynylphenylene substituted zinc and free-base porphyrins. Physical Chemistry Chemical Physics, 13 (4), 1597-1605.

Spectroscopic and computational study of β-ethynylphenylene substituted zinc and free-base porphyrins†

John C. Earles,[a] Keith C. Gordon,*[a] Adam W. I. Stephenson,[b] Ashton C. Partridge[b] and David L. Officer[c]

Received 8th July 2010, Accepted 8th October 2010
DOI: 10.1039/c0cp01113d

A series of tetraphenylporphyrins appended at the β-pyrrolic position with an ethynylphenylene- or ethynylpyridine-substituent have been subjected to spectroscopic and density functional theory (DFT) analyses. The mean absolute deviation between corresponding experimental and DFT-derived vibrational spectra is up to 10.2 cm^{-1}, suggesting that the DFT B3LYP/6-31G(d) method provides an accurate model of the β-substituted porphyrin systems. The configuration interactions that give rise to prominent electronic absorptions have been calculated using time-dependant DFT (TD-DFT) and have been rationalized with reference to the energy and topology of DFT calculated molecular orbitals. As the electron withdrawing capacity of the β-substituent increases the LUMO orbital gains appreciable amplitude over the substituent moiety and is stabilised. This represents a departure from the assumptions underpinning the Gouterman four-orbital model, resulting in atypical electronic absorption spectra. This phenomenon is also manifested in the enhancement patterns of the resonance Raman spectra insofar as B-band excitation engenders an enhancement of substituent based modes. These observations demonstrate that the β-substituent exerts an appreciable electronic influence on the porphyrin π-electron system and provides a means of introducing charge-transfer character to prominent electronic transitions.

1. Introduction

While the literature is replete with examples of substituted mono-porphyrins and porphyrin arrays, there are comparatively few reports of either zinc or free-base porphyrins with β-ethynyl substituents.[1–17] Historically, this is likely to be, at least in part, due to inherent synthetic difficulties associated with this class of compounds. However, recent advances have opened the way for the facile synthesis of β-ethynylphenylene substituted porphyrins that can be readily appended with a wide range of functional groups.[15]

Structurally similar ethenyl-substituted porphyrins have been used to fabricate dye sensitised solar cells (DSSCs) with an overall conversion efficiency of up to 7.1%;[18] an unprecedented result for porphyrin based dyes. In light of this, and the recent remarkable DSSC efficiencies obtained with porphyrin dyes *meso*-substituted with alkynyl linkers,[19] it is of interest to investigate the electronic properties of the relatively new ethynyl analogues. Useful DSSC efficiencies have been shown to be reliant on effective conjugation between the light absorbing porphyrin moiety and the substituent binding group.[17,20] The 'cylindrical' ethynyl-substituent minimises steric strain with neighbouring *meso*-phenyl group, thus facilitating a smaller dihedral angle between the phenyl substituent and the porphyrin plane and, in turn, potentially enhancing conjugation between the two π-electron systems. Ethynyl-substituted porphyrins have previously been incorporated into multi-porphyrin arrays in attempts to create an 'antennae-effect' in which the effective absorption cross-section of a sensitiser is increased.[10,12,13,21] While *meso*-ethynyl linked porphyrins are highly conjugated, with exceptional ground- and excited-state electronic coupling,[12] the β-substituted analogues tend to act as two independent and electronically decoupled porphyrins.[10,12,13] However, this is not necessarily deleterious in terms of DSSC utility: Campbell *et al.*[20] report that a β-substituted mono-porphyrin carboxylic acid derivative with a conjugated linker shows a significant advantage over any of the antennae-type multi-porphyrin arrays for which efficiency data is available.

β-Ethynylphenylene substituted porphyrins have been shown to exhibit charge-transfer (CT) characteristics[3] that can be intensified by appending the substituent with electron withdrawing moieties such as an aldehyde.[11] Electrochemical studies indicate that porphyrin ring oxidation is more facile with β-substituted porphyrins than for the *meso*-substituted analogues.[22] This is attributable, in part, to the electron rich nature of the β-position of the porphyrin core.[23] In addition, an ethynyl β-pyrrolic substituent stabilises the porphyrin ring toward oxidation more effectively than the equivalent ethenyl substituent.[3]

In this study we have employed spectroscopic and computational techniques to investigate the electronic properties of a series of β-ethynyl substituted zinc- and free-base porphyrins

[a] *MacDiarmid Institute for Advanced Materials and Nanotechnology, Department of Chemistry, University of Otago, Dunedin, New Zealand. E-mail: Kgordon@chemistry.otago.ac.nz; Fax: +64 3 479 7906; Tel: +64 3 479 7599*
[b] *IFS MacDiarmid Centre, Massey University, Private Bag 11222, Palmerston North, New Zealand*
[c] *Intelligent Polymer Research Institute, ARC Centre of Excellence for Electromaterials Science, University of Wollongong, Northfields Avenue, Wollongong, NSW 2522, Australia*
† Electronic supplementary information (ESI) available: FT Raman spectra, IR spectra. See DOI: 10.1039/c0cp01113d/

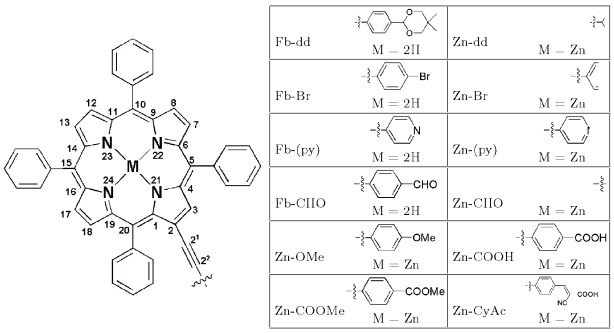

Fig. 1 The atom numbering and naming scheme for all β-substituted porphyrins.

in which the substituent is of varying electron withdrawing strength (Fig. 1). In particular, we have employed resonance Raman (RR) spectroscopy as a means of probing CT character of prominent electronic transitions within the substituted porphyrins. For those molecules in which the substituent bears strong electron withdrawing capacity at the phenyl *para* position, excitation of the porphyrin B-band engenders an enhancement of substituent based vibrational modes. This implies that molecular orbitals with appreciable amplitude over the substituent are prominent in the configuration interactions that give rise to the B-bands. TD-DFT has been employed to model electronic transitions and Mulliken population analyses have been carried out on the resulting configuration interactions. The results show the nature of the substituent affects on both the extent and direction of CT character associated with prominent electronic transitions. These data are rationalised with reference to the calculated molecular orbital energies, specifically, the bearing that these energies have on the Gouterman four-orbital model.[24] β-Ethynyl substitution undermines the assumptions that underpin the Gouterman four-orbital model, leading to a departure from typical porphyrin-like electronic absorption spectra.

2. Experimental

2.1 Computational details

All calculations were performed using Gaussian 03[25] software. Local and non-hybrid methods including LDSA, BP86 and PW91 significantly underestimate the oscillator strengths (*f*) of porphyrin B-bands.[26] However B3LYP has been found to be of comparable accuracy to multireference perturbation theory (PT2) and couple cluster (SAC-CI, CC) methods,[27] whilst being less intensive in terms of computational resources. Previous comparisons between the calculated and experimental ground state electronic spectra of porphyrin systems suggest that hybrid functionals, such as B3LYP, are more accurate over a wider spectral range.[28,29] Furthermore, the B3LYP/6-31G(d) method has been successfully used on similar porphyrin systems to assign prominent peaks in the vibrational spectra.[30–33]

TD-DFT methods have previously been used to model poprhyrin electronic transitions with comparable accuracy to more computationally demanding highly correlated *ab initio* methods.[34] TD-DFT data provide configuration interactions that can be used to rationalize observed electronic phenomena and changes in the distribution of atomic charges associated with electronic excitations. Atomic charges are not a quantum mechanical observable and cannot be predicted from first principles. Consequently, any partitioning scheme is necessarily arbitrary. The Mulliken method assigns the electron density of a particular orbital to the atom on which the orbital is centered. This leads to some shortcomings, particularly when dealing with orbitals of large angular momentum and polar bonds. Notwithstanding these shortcomings, Mulliken population analyses provide a qualitative measure of intramolecular electron distribution that can be very informative. Mulliken population analyses were carried out using GaussSum, version 2.1.6.[35]

Lower level optimisations (B3LYP/3-21g*) were performed on all feasible stereoisomers of the hypothetical molecule [5,10,15,20-tetraphenyl]-2-[2-phenylethynyl]-porphinato zinc(II). The lowest energy calculated structure was that with a 'D_{2d}-like' *meso*-phenyl arrangement (in reference to the point group to which the corresponding ZnTPP structure belongs) and a near co-planar arrangement of the substituent phenyl group with respect to the porphyrin plane. A conformational study on the analogous free-base porphyrins yielded the same results with the additional consideration that the more stable structural isomer is that in which the deprotonated pyrrole bears the β-substituent. Subsequent to this conformational study, all molecules were subjected to higher level (B3LYP/6-31g(d)) computational analyses in the geometric form described above.

2.2 Synthesis

The synthesis of the β-ethynyl-substituted porphyrins was carried out by a modified Horner–Emmons condensation reaction, described in detail elsewhere.[15]

2.3 Physical measurements

Spectrophotometric grade solvents were used for all electronic absorption and resonance Raman measurements. All spectra were analysed using the GRAMS software package (version 5.0, Galactic Industries).

Fourier transform infrared spectra were recorded using a Perkin-Elmer Spectrum BX FT-IR system with Spectrum software (version 2.00). The analyte was pressed into a potassium bromide (KBr) disc; the KBr used for this purpose was kept at approximately 100 °C prior to the formation of the disc, in order to minimise the amount of water present. Spectra were generally recorded from 64 scans, with a resolution of 4 cm^{-1}.

FT-Raman spectra were generally recorded from pure, solid powder samples. In isolated cases, spectra were recorded from a mixture of analyte and KBr in order to prevent the sample from overheating. The spectrometer used was a Bruker IFS-55 FT-interferometer bench equipped with an FRA/106 Raman accessory and a InGaAs D425 or liquid nitrogen cooled Ge D418-T Raman detector. Raman excitation was achieved with 1064 nm light emanating from an Nd : YAG laser with

an operating power of 100 mW. In general, each spectrum was recorded from approximately 100 scans with a resolution of 4 cm^{-1}.

Resonance Raman spectra were recorded from 40–60 μ mol L^{-1} solutions held in a spinning NMR tube. Resonant excitation was achieved using a continuous-wave Innova I-302 krypton-ion laser with an experimental setup described elsewhere.[36,37] Wavelength calibration was performed using Raman bands from a 1 : 1 (by volume) mixture of acetonitrile and toluene. Peak positions were reproducible within 1 cm^{-1}.

Electronic absorption spectra were recorded from 5 μmol L^{-1} solutions at room temperature on a Varian 500 Scan UV-Vis-NIR Spectrophotometer using Cary Win UV Scan Application software. A quartz cell of 1 cm path length was used.

3. Results and discussion

3.1 Geometry and structure

The experimentally[15] and computationally derived bond-lengths for Zn–CHO are depicted in Fig. 2. Substitution at the β-position effects specific structural changes to the porphyrin core, most notably on the substituted pyrrole. These structural changes are attributable to an electronic perturbation of the porphyrin π-system.[33,38] Experimental crystallographic data for Zn–CHO[15] show that bonds C1–C2 and C2–C3 lengthen by 0.9 pm relative to ZnTPP while the C3–C4 bond is shortened by 2.7 pm (Fig. 2, data for ZnTPP taken from Scheidt *et al.*[39]). The same structural deformation is observed to a similar extent in the comparison of ZnTPP with [5,10,15,20-tetraphenyl]-2-[2-(4-pyridinyl)ethenyl]-porphinato zinc(II) (the ethenyl analogue of Zn–(py) (structural data not shown taken from Burrell *et al.*,[40]); suggesting that the ethenyl- and ethynyl-substituents exert a comparable electronic influence on the porphyrin structure.

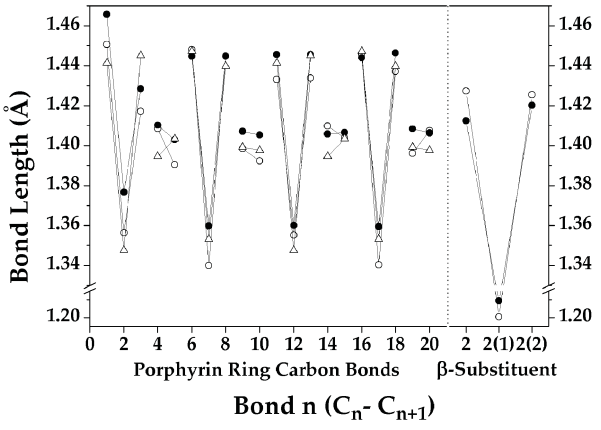

Fig. 2 The bond-lengths for Zn–CHO derived from X-ray diffraction data[15] (○) and the DFT B3LYP/6-31G(d) method (●). The bond lengths for unsubstituted ZnTPP as derived from X-ray diffraction data[39] are included for comparative purposes(△). The bonds are numbered according to Fig. 1 (note that the numbering for ZnTPP necessarily begins at an arbitrary α-carbon owing to the molecular symmetry). The bonds are linked according to their pyrrolic or methine groupings for clarity.

Given the design rationale behind this series of molecules (that is, to increase conjugation between the porphyrin core and substituent), it is of particular interest to examine the relative orientation of the substituent and porphyrin sub-units. As noted by Stephenson *et al.*,[15] the crystal structure of Zn–CHO reveals a dihedral angle between the phenyl and the porphyrin plane of 32°, considerably *less* planar than ethenyl-substituted analogues.[41] However, the substituent phenyl group is well removed from the steric bulk of the porphyrin *meso*-phenyl groups, and, as such, the energetic barrier to rotation about the C≡C bond is likely to be quite low. To test this hypothesis, single point energy calculations were performed at the B3LYP/3-21g* level upon Zn–CHO at ten degree increments throughout the full rotation about the C≡C bond, where the geometrically optimised structure was used as a starting point. The results suggest that the global minimum corresponds to a dihedral angle between the porphyrin plane and the phenyl ring of 0°. Energetic maxima were predicted at ±110° with a relative energy of 3.6 kcal mol^{-1}. The structure with a dihedral angle of 30° was predicted to be 0.78 kcal mol^{-1} less stable than that with one of 0°. It is difficult to compare the extent to which the ethenyl- and ethynyl-motifs facilitate communication between porphyrin and substituent on the strength of these results. However, both substituents are demonstrably conjugated to the porphyrin π-electron system and so meet a requisite criterion for effective sensitisation within a DSSC.[20]

3.2 Raman spectroscopy

3.2.1 FT-Raman spectroscopy. A favourable comparison between the theoretical and experimental spectra indicates that the calculation is a reliable model, while the calculated normal coordinates can in turn be used to assign bands in the vibrational spectra. The correlation between the theoretical and experimental spectra is quantified by the mean absolute deviation (MAD) of corresponding peak frequencies, measured in wavenumbers. The assessment criteria for this study were as follows: all peaks in the experimental spectra that are above a relative intensity of 20% have been identified and related to peaks in the equivalent theoretical spectrum based upon peak position and intensity patterns. A MAD approaching the spectrometer resolution of 4 cm^{-1} represents an excellent correlation between experimental and theoretical spectra. Analysis within this work is confined to the 800 to 2400 cm^{-1} region. The calculated frequencies have been scaled by a factor optimised to yield the lowest MAD for the Raman spectra; this is to compensate for the tendency of DFT methods to overestimate force fields.[42] The scale factors vary between 0.964 and 0.974; this is well within the range routinely employed in DFT studies. The MAD values vary from 4.2 to 11.0 cm^{-1} for the same data set (see Table 1), indicating that the B3LYP/6-31G(d) method provides reliable models of the true systems. The correlation between experimental and theoretical Raman spectra is shown for Zn–CHO in Fig. 3 as a representative example; the calculated data reproduce both the position and general intensity pattern of the observed peaks, allowing for a full assignment of the Raman spectra.

Table 1 The mean absolute deviation (MAD) between experimental and theoretical (B3LYP/6-31G(d)) vibrational data. The scale factors (SF) applied to the calculated spectra are those which minimise the MAD for the Raman spectra

	MAD cm^{-1}		
Molecule	Raman	IR	Scale factor
Fb–dd	7.2	8.4	0.967
Fb–Br	7.6	7.1	0.974
Fb–(py)	9.0	7.0	0.973
Fb–CHO	7.3	8.1	0.965
Zn–dd	9.9	11.0	0.965
Zn–OMe	5.4	7.3	0.964
Zn–Br	8.0	6.4	0.966
Zn–(py)	7.9	8.4	0.964
Zn–COOMe	7.8	6.1	0.965
Zn–CHO	5.7	9.4	0.965
Zn–COOH	4.9	10.4	0.965
Zn–CyAc	6.8	10.3	0.967

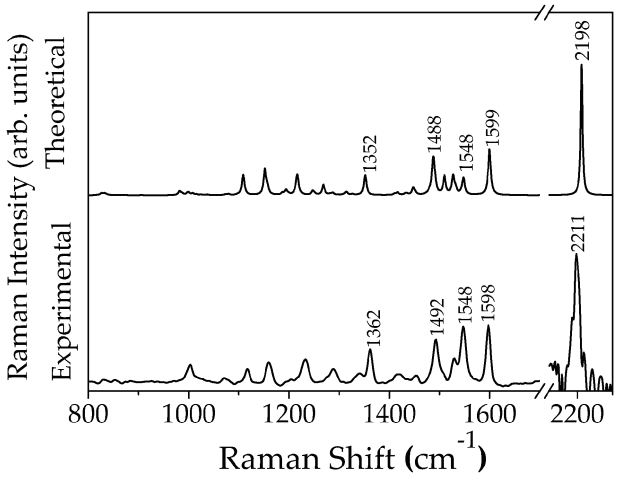

Fig. 3 The correlation between the experimental and theoretical (B3LYP/6-31G(d)) Raman spectra for Zn–CHO.

Let us consider the Fourier transform (FT) Raman spectra, in particular, those of the β-substituted ZnTPP porphyrins (see ESI).† In general, the spectra are remarkably similar. Prominent peaks are observed at ~1003 cm^{-1} (mixed mode), ~1230 cm^{-1} (ν(Pyr. breathing)), ~1360 cm^{-1} (ν(Pyr. half-ring)$_{sym}$ or 'ν_4'), ~1490 cm^{-1} (mixed mode), ~1550 cm^{-1} (ν(C_β–C_β)) and ~1600 cm^{-1} (ϕ(substituent)); note that the nomenclature used to describe vibrational modes is that adopted by Li *et al.*[43] The calculated vibrational modes are often heavily mixed, but are generally very consistent across the series of molecules. There is a prominent peak observed in all Raman spectra at ~2200 cm^{-1}, corresponding to ν(C≡C); this mode remains strong and unmoved across the series. Many of the above observations hold true when considering the FT-Raman spectra of the β-substituted free base porphyrins (see ESI)†: there are only subtle differences across the spectra, and the prominent modes are in similar positions to the zinc analogues. The most notable exception is the ν_4 band, which shifts from ~1360 cm^{-1} for the zinc porphyrin series to a less intense band at ~1380 cm^{-1} for the free base porphyrins.

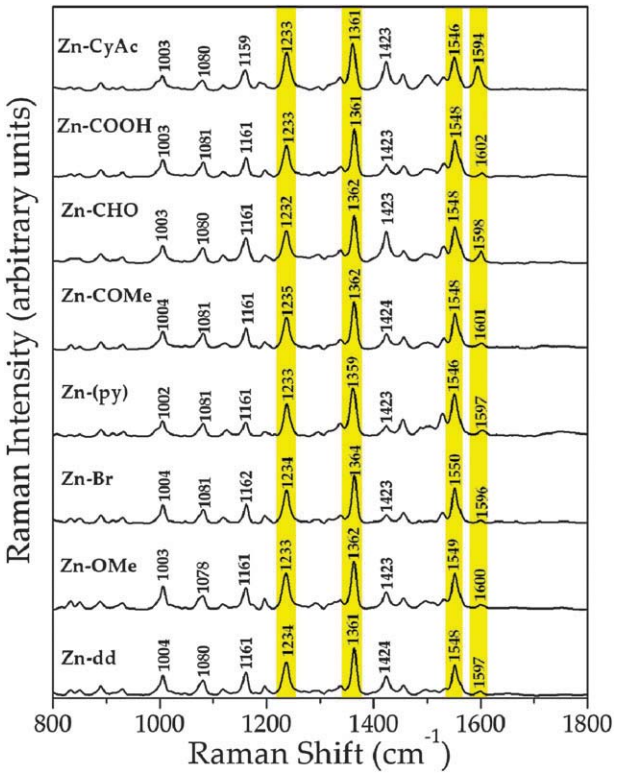

Fig. 4 The experimental resonance Raman spectra for β-substituted zinc porphyrins. The spectra were recorded from $4 - 6 \times 10^{-5}$ mol L^{-1} solutions in dichloromethane using an excitation wavelength of 413 nm. Bands that are discussed in the text have been highlighted.

3.2.2 Resonance Raman spectroscopy. Resonant excitation of the porphyrin B-band gives rise to a strong enhancement of the Raman signals from modes which posses A_{1g} symmetry.[33,43] The 413 nm excited resonance Raman (RR) spectra for the β-substituted zinc porphyrins are shown in Fig. 4. Bands that are noticably enhanced include those at ~1230 cm^{-1} (ν(Pyr. breathing)), ~1360 cm^{-1} (ν(Pyr. half-ring)$_{sym}$, or 'ν_4')

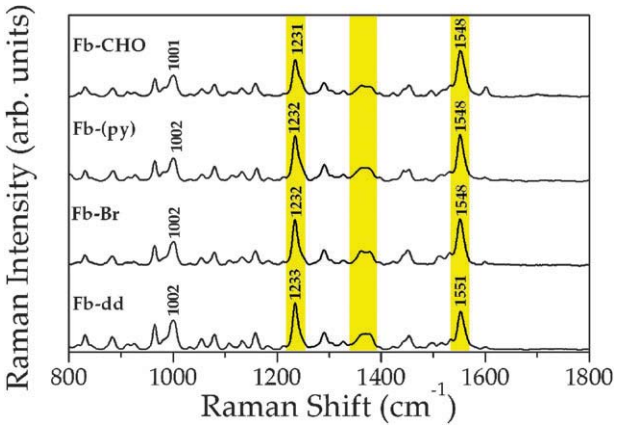

Fig. 5 The experimental resonance Raman spectra for β-substituted free-base porphyrins. The spectra were recorded from 5–8 × 10^{-5} mol L^{-1} solutions in dichloromethane using an excitation wavelength of 413 nm. Bands that are discussed in the text have been highlighted.

and ~1550 cm^{-1} ($\nu(C_\beta–C_\beta)$). The analogous modes are enhanced in the spectra of the free-base porphyrins (Fig. 5), the ν_4 mode observed at ~1380 cm^{-1} in the FT-Raman spectra is broadened over 1360–1380 cm^{-1}.

The substituent based mode in the 1594–1602 cm^{-1} region is less prominent in the RR spectra than it is in the corresponding FT-Raman spectra, for all porphyrins. The electronic transition that occurs at 413 nm (corresponding to the B-band) involves predominantly porphyrin-centred orbitals and, as such, does not engender an excitation of substituent based modes. However, this observation is not uniformly applicable. The substituent based mode of Zn–CyAc at 1594 cm^{-1} is noticeably more intense than other such modes (see Fig. 4). One can deduce from this that the configuration interaction that gives rise to the B-band electronic transition of Zn–CyAc involves a significant contribution from substituent-based orbitals. There are two explanations for this: firstly the LUMO gains significantly more substituent character as the electron withdrawing capacity of the substituent increases and secondly, the substituent based HOMO-2 and LUMO + 2 orbitals become involved in the resonant configuration interaction. These phenomena are discussed with reference to TD-DFT calculated electronic transitions and orbital data shortly.

3.3 Infrared spectroscopy

The infrared spectra of all β-substituted zinc porphyrins are shown in the ESI.† The porphyrin core modes do not differ appreciably over the series, giving rise to a similar spectral pattern. There are however noticeable differences in the IR spectra arising from the various substituent based modes. Molecules with ether functionality have C$^-$O$^-$C stretching modes, observed at 1100, 1246 and 1274 cm^{-1} for Zn–dd, Zn–OMe and Zn–COOMe, respectively. Similarly, C=O stretching modes are observed at approximately 1700 cm^{-1}. This is also true of the β-substituted free base-porphyrins (see ESI)†: in general the IR spectra are similar excepting that Fb–dd and Fb–CHO have intense substituent based modes at 1100 and 1700 cm^{-1}, respectively.

The IR spectra of all the porphyrins show a weak $\nu(C\equiv C)$ stretching mode in the region from 2193–2202 cm^{-1}. The relative intensities of this mode relate to the electron withdrawing strength of the substituent. Having groups of highly disparate electron affinity either side of the C≡C bond breaks the symmetry across the bond that ordinarily precludes an appreciable IR signal; this is most apparent in the IR spectra of Zn–(py), Zn–CyAc, Fb–(py) and Fb–CHO.

3.4 UV-visible spectroscopy and time-dependent DFT

The UV-visible spectra for all β-substituted porphyrins are shown in Fig. 6. In general, they are typical porphyrin spectra with intense B-bands and weaker Q-bands. The spectra corresponding to the free-base porphyrins (Fig. 6a) exhibit four distinct Q-bands. Metal complexation increases the ring micro-symmetry from D_{2h} to D_{4h}[3,44] and has with it an associated decrease in the number of Q-bands from four to two.

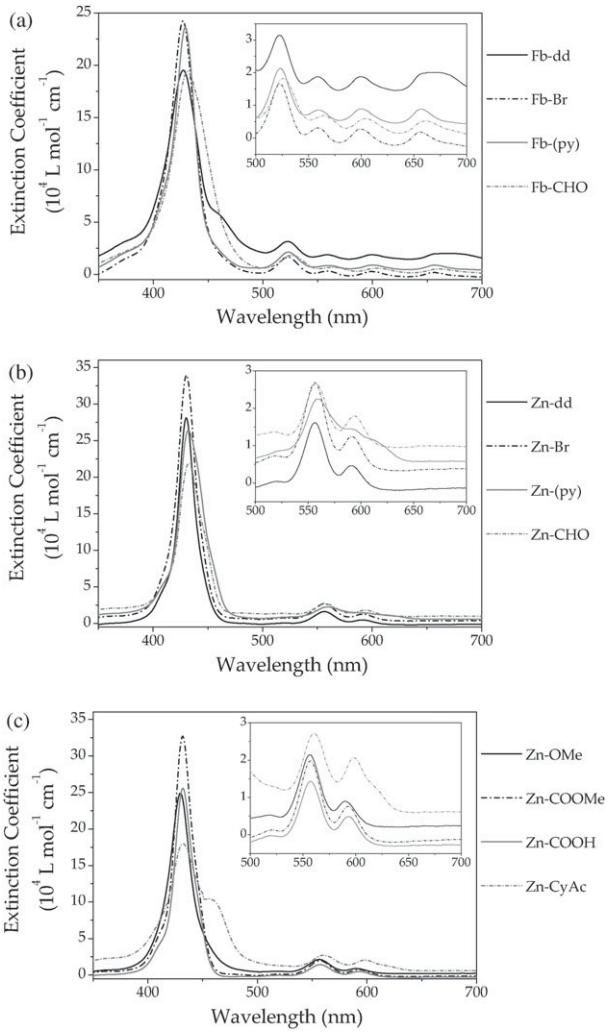

Fig. 6 The experimental UV-visible spectra for all β-substituted porphyrins, taken from 5 × 10^{-6} mol L^{-1} solutions in CH_2Cl_2. The intensities have been baseline corrected against CH_2Cl_2. The insets are rescaled in order to better depict the weaker Q-bands. (a) β-Substituted free-base porphyrins, (b) β-substituted zinc porphyrins (those with free-base analogues), (c) β-substituted zinc porphyrins (those without free-base analogues).

The Gouterman four-orbital model[24] predicts that both the B- and Q-bands are comprised of transitions involving the four frontier MO's (HOMO-1 through to LUMO + 1). The model is based on the assumption that the four frontier MO's are energetically isolated, that is, the two HOMO's are themselves close in energy but markedly different to the nearest MO's in either direction, as with the two LUMO's. Fig. 7 contains the calculated molecular orbital energies for all β-substituted porphyrins under consideration, and their unsubstituted analogues. The four frontier MO's of the unsubstituted porphyrins are indeed isolated, with 1.0–1.5 eV separating them from the HOMO-2 and LUMO + 2 orbitals. However upon substitution these neighbouring orbitals become much closer in energy, leading to a departure from typical Gouterman behaviour.

The HOMO-2 orbitals of the molecules in this study have no spatial analogue in either unsubstituted FbTPP or ZnTPP,

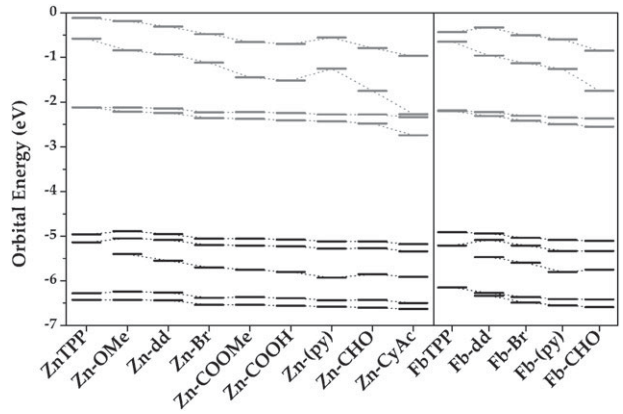

Fig. 7 The calculated molecular orbital energies for all β-substituted porphyrins. The molecules are arranged such that the LUMO decreases in energy from left to right, within each grouping (Zn- and Fb- porhyrins), that is, they are arranged according to the electron withdrawing strength of the substituent. Occupied and unoccupied orbitals are depicted in black and gray, respectively. The data were calculated using the B3LYP/6-31G(d) method.

as they are largely substituent based (see Table 2), yet they are close enough in energy to the two HOMOs to be heavily involved in the configuration interaction that gives rise to the prominent porphyrin absorptions. This is reflected in the TD-DFT calculated configuration interactions (Table 3), with the HOMO-2 orbital heavily involved in all B-band transitions. Moreover, they are involved in an electron donating capacity, suggesting that the B-band transition may have associated substituent to porphyrin CT character (discussed further in section 3.6).

Considering the unoccupied MO's, the substituent based LUMO + 2 is closest in energy to the LUMO + 1 for those molecules with a relatively electron withdrawing substituent, most notably Fb–CHO and Zn–CyAc (see Fig. 7). Accordingly, the LUMO + 2 is involved in the calculated configuration interactions that give rise to the B-bands for these particular molecules (Table 3), moreover, it is involved in an accepting capacity.

Another key assumption underpinning the Gouterman four-orbital model is that the HOMO and HOMO-1, as well as the LUMO and LUMO + 1 are nearly degenerate. The calculated MO energies (Fig. 7) show that for the unsubstituted porphyrins ZnTPP and FbTPP the two LUMO's are degenerate, while the two HOMO's are near degenerate. Substitution does not affect the relative energies of the two HOMO's markedly. However, the degeneracy of the two LUMO's is broken, owing to the differing orbital amplitudes on the substituted β-carbon.

Substitution at the β-carbon has been shown to affect the electronic structure of the porphyrin π-system such that the assumptions on which the Gouterman four-orbital model is based are less applicable. While this does not lead to a wholesale alteration of the UV-visible spectra, it does have some tangible effects; most notably, the B-bands become broader. The FWHM values vary in a manner that is commensurate with the electron withdrawing ability of the substituent. That is to say, more electron withdrawing substituents lead to a greater departure from the 'Gouterman-type' behaviour and thus broader B-bands. For example, the widest and least intense B-bands are observed for Fb–CHO and Zn–CyAc, which in turn have the most delocalised calculated molecular orbitals (Table 2). Conversely, the B-bands of Fb–Br and Zn–Br, for example, are relatively narrow and intense, a result of the relatively unperturbed, more 'porphyrin-like' orbitals.

Ethynyl substitution at the β-position has effected a bathochromic shift in the B-band absorptions. Unsubstituted FbTPP and ZnTPP have a λ_{max} of 420 and 419 nm respectively in CH_2Cl_2.[45] The corresponding values for this study are 427–431 nm for free-base and 430–433 nm for ZnTPP molecules (see Table 3). Similarly, the Q-bands are red-shifted relative to the unsubstituted analogues. Walsh *et al.*[45] report

Table 2 Calculated molecular orbital representations for Zn–Br and Zn–CyAc—the zinc porphyrins on which the substituent has the least and greatest electron withdrawing capacity, respectively. The ratio of electron density over the porphyrin to that over the substituent moiety is given for each orbital (as calculated by Mulliken population analyses). The unsubstituted ZnTPP analogue is included for comparative purposes. Calculated using the B3LYP/6-31G(d) method

MO	ZnTPP	Zn–Br	Zn–CyAc
L + 2		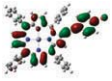 52:48	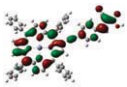 63:37
L + 1		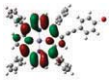 100:0	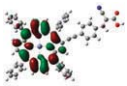 99:1
LUMO		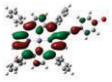 91:9	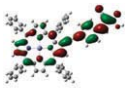 39:61
HOMO		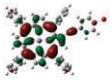 93:7	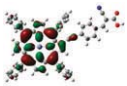 96:4
H-1		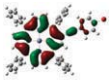 90:10	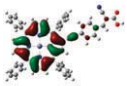 91:9
H-2		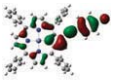 51:49	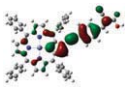 47:53

Table 3 Correlation between experimental and theoretical Soret/B-band electronic transitions. Each transition is comprised of a configuration interaction of many one-electron transitions between molecular orbitals; the calculated weighting of each transition in the final configuration is given. The calculated electron distribution of the excited electron over the porphyrin moiety is given for the initial and final states (the unaccounted electron density is over the substituent moiety). The experimental electronic absorption spectra were taken from 5×10^{-6} mol L^{-1} solutions in CH_2Cl_2, computational data were calculated using Time-dependent DFT, at the B3LYP/6-31G(d) level

	Experimental			Calculated					
							Configuration interaction		Electron distribution
Molecule	λ/nm	E/eV	Extinction coefficient/ mol $L^{-1}cm^{-1}$	λ/nm	E/eV	f	$D \rightarrow A$, coefficient	$D \rightarrow A$, coefficient	$i \rightarrow f$ (Δ) (%)
Fb–dd	427	2.90	195000	389	3.19	1.75	H-2 → LUMO, 17%	HOMO → L+1, 14%	78 → 94 (16)
	458(sh)	2.71	59200	393	3.15	0.66	H-3 → LUMO, 18%	H-2 → L+1, 17%	82 → 94 (12)
Fb–(py)	429	2.89	236000	392	3.17	1.42	H-2 → LUMO, 13%	H-1 → LUMO, 16%	82 → 88 (6)
Fb–Br	427	2.90	243000	391	3.17	1.66	H-2 → LUMO, 16%	HOMO → L+1, 14%	78 → 90 (12)
Fb–CHO	431	2.88	194000	410	3.03	0.97	H-2 → LUMO, −22%	H-1 → L+2, 36%	78 → 61 (−17)
Zn–dd	430	2.88	281000	451	2.75	0.72	H-2 → LUMO, 56%	H-1 → LUMO, 17%	68 → 93 (25)
Zn–OMe	430	2.88	249000	471	2.63	0.56	H-2 → LUMO, 51%	H-1 → LUMO, 15%	71 → 94 (23)
Zn–Br	430	2.88	339000	445	2.79	0.80	H-2 → LUMO, 55%	H-1 → LUMO, 17%	66 → 92 (26)
Zn–(py)	432	2.87	264000	426	2.91	0.98	H-2 → LUMO, 44%	H-1 → LUMO, 20%	73 → 92 (19)
Zn–COOMe	432	2.87	327000	441	2.81	1.05	H-2 → LUMO, 49%	H-1 → LUMO, 19%	69 → 89 (20)
Zn–CHO	433	2.86	219000	442	2.81	1.25	H-2 → LUMO, 37%	H-1 → LUMO, 21%	74 → 83 (9)
Zn–COOH	432	2.87	256000	440	2.82	1.10	H-2 → LUMO, 46%	H-1 → LUMO, 19%	70 → 89 (19)
Zn–CyAc	431	2.88	180000	446	2.78	0.76	H-2 → LUMO, 66%	H-1 → L+2, −18%	57 → 45 (−12)
	455	2.72	105000	491	2.52	0.63	H-1 → LUMO, 29%	H-1 → L+2, 34%	93 → 66 (−27)

Q-bands for FbTPP at 514, 548, 589 and 646 nm. The Q-bands of the β-ethynyl substituted free-base porphyrins are 9–25 nm to the red of these values, corresponding to a decrease in energy of 236–577 cm^{-1}. In addition, Walsh *et al.*[45] report Q-bands for ZnTPP at 548 and 589 nm. The substituted zinc porphyrins of this study absorb up to 11 nm further to the red, corresponding to an energy shift of up to 359 cm^{-1}. These results suggest that the ethynyl substituent has an overall electron withdrawing effect on the porphyrin core.[33]

3.5 Molecular orbital analysis

The calculated frontier molecular orbitals for free base and zinc β-substituted porphyrins are depicted in Table 2. The porphyrin centred orbitals are spatially comparable to those of the unsubstituted analogues FbTPP and ZnTPP, enabling direct comparisons to be made. The two e_g symmetric LUMO's differ only in that they are aligned at 90° to one another, for both FbTPP and ZnTPP. This gives rise to the degeneracy shown in Fig. 7. However, it also creates a large discrepancy in the orbital distribution over the substituted β-carbon. Where the molecular orbital has negligible amplitude on the substituted β-carbon, it is largely unperturbed relative to the 'parent' porphyrin (for example, the LUMO+1 orbitals). Conversely, where the substituted carbon is electron rich the orbitals are heavily delocalised and so stabilised, as occurs in the LUMO orbitals. This breaks the degeneracy and leads to a departure from the Gouterman four-orbital model in the UV-visible spectra, as described above.

As the electron withdrawing strength of the *para*-substituent increases the LUMO orbitals gain progressively more amplitude over the substituent moiety. For example, Mulliken population analysis suggests that the LUMO of Zn–Br is partitioned over the porphyrin and substituent moieties at a ratio of 91 : 9, while that of Zn–CyAc is distributed at 39 : 61, that is, it has a higher amplitude over the substituent than the porphyrin core (see Table 2).

3.6 Mulliken population analysis

Mulliken population analysis, as implemented by the GaussSum software package,[35] has been used to quantify the change in electron distribution over the porphyrin and substituent moieties that is associated with TD-DFT calculated B-band transitions. In this manner, one is able to quantify the CT character associated with the calculated transition. The results of this analysis are given in Table 3. The calculated B-band electronic transitions for all molecules, except Zn–CyAc and Fb–CHO, indicate an electron redistribution from the substituent toward the porphyrin core. For example, consider Zn–Br, the relevant electron (that is, the electron that is excited) resides over the porphyrin moiety 66% of the time in the ground state and 92% in the excited state. The configuration interaction underpinning this transition is comprised of significant (55%) HOMO-2 → LUMO character. Here the substituent based HOMO-2 and the porphyrin based LUMO are acting in a donating and accepting capacity, respectively, hence the substituent to porphyrin CT character. Conversely, the electron redistribution associated with the B-bands of Zn–CyAc and Fb–CHO is from porphyrin to substituent. This is a result of previously mentioned phenomena: the LUMO gains progressively more amplitude over the substituent moiety as the electron withdrawing capacity increases and the substituent based LUMO+2 features prominently in the configuration interaction in an accepting capacity.

4. Conclusions

DFT has been used to determine the lowest energy conformers of the various β-phenylethynyl substituted ZnTPP and FbTPP porphyrins. From these structures a series of computational analyses have been performed. The geometric distortion to the porphyrin core effected by the β-ethynyl substituent is comparable to that effected by analogous β-ethenyl substituents,

indicating that each is conjugated to the porphyrin π-system to a similar extent.

There is an excellent correlation between theoretically and experimentally derived vibrational spectra. This suggests that the B3LYP/6-31G(d) computational method is well suited to these types of molecules. Certain vibrational modes are particularly sensitive to metallation and the associated changes in porphyrin core size. The UV-visible spectra, in general, show typical porphyrin behaviour. However there are subtle variations in band-width and intensity that can be explained in terms of a departure from the idealised 'Gouterman type' orbital scenario. This interpretation is in accordance with the DFT calculated orbital energies and topologies.

The β-ethynyl substituent has an overall electron withdrawing effect on the porphyrin macro-cycle;[33] the extent of this influence varies with the different substituents. This is manifested in a number of calculated and experimental analyses. The calculated orbital energies (Fig. 7) reflect the extent of orbital delocalisation over the porphyrin and substituent sub-units depicted in Table 2, insofar as molecules with delocalised orbitals are stabilised to a greater extent. Experimentally, this is manifested in the UV-visible spectra (the FWHM of the B-band and intensity of the B-band relative to the Q-bands), resonance Raman spectra (the intensity of substituent based vibrational modes) and the infrared spectra (the intensity of the $\nu(C\equiv C)$ stretching mode). TD-DFT data indicate that the electron withdrawing strength of the substituent can influence the direction of the electron density changes across the porphyrin and substituent sub-units that are associated with electronic absorptions. These results demonstrate that the electronics of the porphyrin core can be modified in a predictable and controlled manner.

References

1 D. P. Arnold and L. J. Nitschinsk, *Tetrahedron*, 1992, **48**, 8781–92.
2 P. J. Angiolillo, V. S.-Y. Lin, J. M. Vanderkooi and M. J. Therien, *J. Am. Chem. Soc.*, 1995, **117**, 12514–27.
3 E. Annoni, M. Pizzotti, R. Ugo, S. Quici, T. Morotti, M. Bruschi and P. Mussini, *Eur. J. Inorg. Chem.*, 2005, 3857–3874.
4 H. J. Callot, *B. Soc. Chim. Fr.*, 1974, **7–8**(Pt. 2), 1492–6.
5 T. Chandra, B. J. Kraft, J. C. Huffman and J. M. Zaleski, *Inorg. Chem.*, 2003, **42**, 5158–5172.
6 E. Collini, S. Mazzucato, M. Zerbetto, C. Ferrante, R. Bozio, M. Pizzotti, F. Tessore and R. Ugo, *Chem. Phys. Lett.*, 2008, **454**, 70–74.
7 J. T. Fletcher and M. J. Therien, *J. Am. Chem. Soc.*, 2002, **124**, 4298–4311.
8 J. T. Fletcher and M. J. Therien, *J. Am. Chem. Soc.*, 2000, **122**, 12393–12394.
9 B. Koenig and H. Zieg, *Synthesis*, 1998, 171–174.
10 R. Kumble, S. Palese, V. S.-Y. Lin, M. J. Therien and R. M. Hochstrasser, *J. Am. Chem. Soc.*, 1998, **120**, 11489–11498.
11 A. Lembo, P. Tagliatesta and D. M. Guldi, *J. Phys. Chem. A*, 2006, **110**, 11424–11434.
12 V. S.-Y. Lin and M. J. Therien, *Chem.–Eur. J.*, 1995, **1**, 645–51.
13 V. S. Y. Lin, S. G. DiMagno and M. J. Therien, *Science*, 1994, **264**, 1105–11.
14 C. S. Nash, *J. Chem. Theory Comput.*, 2005, **1**, 261–266.
15 A. W. I. Stephenson, P. Wagner, A. C. Partridge, K. W. Jolley, V. V. Filichev and D. L. Officer, *Tetrahedron Lett.*, 2008, **49**, 5632–5635.
16 S. A. Vail, D. I. Schuster, D. M. Guldi, M. Isosomppi, N. Tkachenko, H. Lemmetyinen, A. Palkar, L. Echegoyen, X. Chen and J. Z. H. Zhang, *J. Phys. Chem. B*, 2006, **110**, 14155–14166.
17 C. W. Lee, H. P. Lu, C. M. Lan, Y. L. Huang, Y. R. Liang, W. N. Yen, Y. C. Liu, Y. S. Lin, E. W. G. Diau and C. Y. Yeh, *Chem.–Eur. J.*, 2009, **15**, 1403–1412.
18 W. M. Campbell, K. W. Jolley, P. Wagner, K. Wagner, P. J. Walsh, K. C. Gordon, L. Schmidt-Mende, M. K. Nazeeruddin, Q. Wang, M. Graetzel and D. L. Officer, *J. Phys. Chem. C*, 2007, **111**, 11760–11762.
19 S. L. Wu, H. P. Lu, H. T. Yu, S. H. Chuang, C. L. Chiu, C. W. Lee, E. W. G. Diau and C. Y. Yeh, *Energy Environ. Sci.*, 2010, **3**, 949–955.
20 W. M. Campbell, A. K. Burrell, D. L. Officer and K. W. Jolley, *Coord. Chem. Rev.*, 2004, **248**, 1363–833.
21 J. J. Gosper and M. Ali, *J. Chem. Soc., Chem. Commun.*, 1994, 1707–8.
22 A. Sen and V. Krishnan, *Tetrahedron Lett.*, 1996, **37**, 8437–8438.
23 I. D. L. Albert, T. J. Marks and M. A. Ratner, *Chem. Mater.*, 1998, **10**, 753–762.
24 M. Gouterman, G. Wagniere and L. C. Snyder, *J. Mol. Spectrosc.*, 1963, **11**, 108–27.
25 M. J. Frisch, G. W. Trucks, H. B. Schlegel, G. E. Scuseria, M. A. Robb, J. R. Cheeseman, J. A. Montgomery, Jr., T. Vreven, K. N. Kudin, J. C. Burant, J. M. Millam, S. S. Iyengar, J. Tomasi, V. Barone, B. Mennucci, M. Cossi, G. Scalmani, N. Rega, G. A. Petersson, H. Nakatsuji, M. Hada, M. Ehara, K. Toyota, R. Fukuda, J. Hasegawa, M. Ishida, T. Nakajima, Y. Honda, O. Kitao, H. Nakai, M. Klene, X. Li, J. E. Knox, H. P. Hratchian, J. B. Cross, V. Bakken, C. Adamo, J. Jaramillo, R. Gomperts, R. E. Stratmann, O. Yazyev, A. J. Austin, R. Cammi, C. Pomelli, J. W. Ochterski, P. Y. Ayala, K. Morokuma, G. A. Voth, P. Salvador, J. J. Dannenberg, V. G. Zakrzewski, S. Dapprich, A. D. Daniels, M. C. Strain, O. Farkas, D. K. Malick, A. D. Rabuck, K. Raghavachari, J. B. Foresman, J. V. Ortiz, Q. Cui, A. G. Baboul, S. Clifford, J. Cioslowski, B. B. Stefanov, G. Liu, A. Liashenko, P. Piskorz, I. Komaromi, R. L. Martin, D. J. Fox, T. Keith, M. A. Al-Laham, C. Y. Peng, A. Nanayakkara, M. Challacombe, P. M. W. Gill, B. Johnson, W. Chen, M. W. Wong, C. Gonzalez and J. A. Pople, *GAUSSIAN 03, Revision C.02*, Gaussian, Inc., Wallingford, CT, 2004.
26 Q. Wang, W. M. Campbell, E. E. Bonfantani, K. W. Jolley, D. L. Officer, P. J. Walsh, K. Gordon, R. Humphry-Baker, M. K. Nazeeruddin and M. Graetzel, *J. Phys. Chem. B*, 2005, **109**, 15397–15409.
27 K. A. Nguyen, P. N. Day and R. Pachter, *J. Phys. Chem. A*, 2000, **104**, 4748–4754.
28 K. A. Nguyen, P. N. Day and R. Pachter, *J. Chem. Phys.*, 1999, **110**, 9135–9144.
29 S. J. A. van Gisbergen, A. Rosa, G. Ricciardi and E. J. Baerends, *J. Chem. Phys.*, 1999, **111**, 2499–2506.
30 P. M. Kozlowski, I. Rush, S. Thomas, A. A. Jarzecki, M. Z. Zgierski, B. Chase, C. Piffat, B.-H. Ye, X.-Y. Li, P. Pulay and T. G. Spiro, *J. Phys. Chem. A*, 1999, **103**, 1357–1366.
31 R. E. Oakes and S. E. J. Bell, *J. Phys. Chem. A*, 2003, **107**, 10953–10959.
32 R. E. Oakes, S. J. Spence and S. E. J. Bell, *J. Phys. Chem. A*, 2003, **107**, 2964–2973.
33 P. J. Walsh, K. C. Gordon, P. Wagner and D. L. Officer, *ChemPhysChem*, 2006, **7**, 2358–2365.
34 E. Baerends, G. Ricciardi, A. Rosa and S. van Gisbergen, *Coord. Chem. Rev.*, 2002, **230**, 5–27.
35 N. M. O'Boyle, A. L. Tenderholt and K. M. Langner, *J. Comput. Chem.*, 2008, **29**, 839–845.
36 R. Horvath, C. A. Otter, K. C. Gordon, A. M. Brodie and E. W. Ainscough, *Inorg. Chem.*, 2010, **49**, 4073–4083.
37 S. J. Lind, K. C. Gordon, S. Gambhir and D. L. Officer, *Phys. Chem. Chem. Phys.*, 2009, **11**, 5598–607.
38 P. J. Walsh, K. C. Gordon, D. L. Officer and W. M. Campbell, *J. Molec. Struct.: Theochem*, 2006, **759**, 17–24.

39 W. R. Scheidt, M. E. Kastner and K. Hatano, *Inorg. Chem.*, 1978, **17**, 706–10.
40 A. K. Burrell, D. L. Officer, D. C. W. Reid and K. Y. Wild, *Angew. Chem., Int. Ed.*, 1998, **37**, 114–117.
41 A. K. Burrell, D. L. Officer and D. C. W. Reid, *Angew. Chem., Int. Ed. Engl.*, 1995, **34**, 900–2.
42 A. P. Scott and L. Radom, *J. Phys. Chem.*, 1996, **100**, 16502–16513.
43 X. Y. Li, R. S. Czernuszewicz, J. R. Kincaid, Y. O. Su and T. G. Spiro, *J. Phys. Chem.*, 1990, **94**, 31–47.
44 M. Gouterman, *J. Mol. Spectrosc.*, 1961, **6**, 138–63.
45 C. J. Walsh, T. Sooksimuang and B. K. Mandal, *J. Porphyrins Phthalocyanines*, 2001, **5**, 803–805.